PHYSICAL REVIEW E **77**, 031504 (2008)

Asymptotic analysis of ion transport in a nonlinear regime around polarized electrodes under ac

Y. K. Suh[1,*] and S. Kang[1]

[1]*Department of Mechanical Engineering, Dong-A University, 840 Hadan-dong, Saha-gu, Busan 604-714, Korea*

(Received 11 October 2007; revised manuscript received 27 January 2008; published 13 March 2008)

In this paper we present the asymptotic solutions of the Poisson-Nernst-Planck equations describing ion transport near a polarized electrode under ac. The solutions can be described in terms of the triple-layer (or quadruple-layer in the transient period) structure. In the thinnest inner layer outside the Stern layer, cations and anions show alternating charging with the same frequency as ac. Next to the inner layer is a buffer region or "middle layer" in which cations and anions exhibit the same behavior but with a frequency double that of the ac frequency. The outer layer shows quasisteady diffusion of ions expanding toward the bulk region and vanishes after the transient period. The potential drop occurs only through the inner layer, which together with the concentrations can be obtained by solving a simple dynamical equation. The asymptotic method is applied to the one-dimensional ion-transport within two parallel facing electrodes and the solutions compare well with the ones obtained with robust numerical methods for the original full equations at various ranges of parameters. We also considered the effect of ion adsorption at the interface between the Stern and inner layers on the ion transport and the virtual slip velocity for the case of facing electrodes.

DOI: 10.1103/PhysRevE.77.031504 PACS number(s): 82.45.Mp

I. INTRODUCTION

It is well known that a solid surface when in contact with an electrolyte is usually negatively charged so that the counterions in the electrolyte are attracted to and the coions are repelled from the interface. The thin layer near the interface showing such unbalanced distribution of ions is called the electrical double layer (EDL), and it is known to be composed of basically two layers. The innermost layer, called the Stern layer, is free of charge and almost motionless because of the strong electrical force exerted from the solid wall. The remaining one, called the diffuse layer, has more cations than anions. When an electric field is externally applied parallel to the interface, the mobile cations and anions in the diffuse layer tend to move toward the cathode and anode, respectively. Since more cations than anions are distributed in the layer, the overall effect is that a fluid flow toward the cathode is induced. The fluid velocity at the edge of the diffuse layer is calculated by using the well known Helmholtz-Smoluchowski equation. Since in microfluidic devices the fluid is confined in a space with small length scales, the bulk fluid out of the EDL is pulled immediately by the edge velocity, and for the channel case the velocity profile takes a plug-type form. This effect is called the dc electroosmosis [1].

The electroosmosis described above is an example of the EDL effect under a dc electric field. Very recently, however, increased attention has been given to the application of ac electric field in the microfluidic flow and particle controls. In this case, the dynamic phenomena of ion transport in the thin layer on the electrode receiving an ac electric field drive the fluid motion. The response of the layer to ac is more interesting and of course more dynamic than dc. The forcing frequency serves as another control parameter, and so ac is more feasible to use than dc. Further, the electrode life becomes longer with ac. Use of ac in controlling particle assembly in small devices has been discussed recently by several research groups. Trau *et al.* [2] showed the long-range attraction of 2-μm-size particles on indium-tin oxide (ITO) electrodes, and they attributed such phenomenon to the hydrodynamic force exerted by the induced charge on the electrode. Green's group [3,4] reported separation of submicrometer particles on the array of electrodes, and they conjectured that heat generation and the subsequent gradient of the conductivity and permittivity of the medium may induce the hydrodynamic force which produces the particle motion. Later, they introduced the concept of ac electric-field-induced flow and electrode polarization to explain their experimental findings and proposed a simple capacitor model to verify the magnitude of the measured velocity [5]. However, the predicted velocity turned out to be much greater than the measured one. Another research group [6] attempted to fit the data of the Green's group with their theoretical model [7] without success. Later Green *et al.* [8] refined their capacitor model by introducing another parameter representing the effect of potential drop across the compact (Stern) layer.

Much of experimental evidence of the ac electroosmosis has been further reported in association with particle migration and assembly. Wong *et al.* [9,10] fabricated a circular electrode surrounded by a circular strip of counter electrode and used PIV (particle image velocimetry) to measure the fluid velocity induced by the ac electroosmosis. The measured velocity shows its dependence on the frequency and the electrolyte concentration. They also demonstrated the trapping of DNA molecules. Brown and Meinhart [11] also conducted a DNA-concentration experiment with a very similar electrode arrangement as that of Wong *et al.* [9]. Their numerical results were, however, two orders of magnitude greater than the measured ones, and the predicted optimum frequency, at which the velocity becomes maximum, was also more than two orders of magnitude smaller than the experimental ones. Several experiments on the evidence of particle aggregation along the center of electrode strip have

---

[*] Correspondig author. FAX: 82-51-200-7656. yksuh@dau.ac.kr

also been reported [12–15]. Bhatt *et al.* [16] demonstrated the collection and concentration of latex particles and yeast cells around the patterned electrodes. Wong *et al.* [9] reviewed various electrokinetic effects and their application in biotechnology. The ac electroosmotic effect is mostly combined with the dielectrophoretic effect in control of the particles (e.g. [17,18]).

The ac electroosmotic phenomena can be applied to various fields of microfluidics. Mpholo *et al.* [19] showed that the plug-type flow profile can be achieved by placing two anisotropic arrays of electrodes in pumping fluid in a channel. Studer *et al.* [20] presented a fabrication method for the pumping device using ac electroosmosis. In order to pump fluid by using the ac electroosmotic effect, breaking of symmetry in the electric field (usually by using asymmetric geometry in the shape of electrodes themselves or in their arrays) is necessary. Bazant and Squires [21] and Squires and Bazant [22] gave examples of electrode arrays for such purposes. The ac electroosmosis can also be used in fluid mixing. Wang *et al.* [23] exhibited a turbulent-like mixing within a chamber containing small conductive granules by applying dc and ac fields. They attributed the enhanced mixing to the vortices around the granules caused by the induced charge electroosmosis, as predicted by Bazant and Squires [21]. On the other hand, Wu *et al.* [14] observed asymmetric flow patterns even with the symmetric electrode configuration, and they explained the phenomenon in terms of asymmetric-polarization, in which the Faraday reaction is to occur on the electrodes.

The basic ingredient of the above ac electroosmotic phenomena is the ion transport within the layer, and this is decoupled from the fluid-flow problem because the ion transport given by the convection can be neglected in most practical cases. So, the very beginning point of the fundamental study on the ac electroosmosis should be the analysis of the ion transport in the layer. The governing equations for the ion transport within the layer are the Poisson-Nernst-Planck equations, which describe the conservation of ions (Nernst-Planck equation) and the relation between the electrical potential and charge density (Poisson equation). As widely surveyed by Bazant *et al.* [24], theoretical treatment of the Nernst-Planck equation goes back to Helmholtz. Since then the electrical effect of the layer on the bulk electrolyte has been studied in terms of the development of an electrical circuit model or simply the capacitor model representing the relation between the accumulation of charge in the layer and the potential drop across the EDL (refer to the literature given by Bazant *et al.* [24] for the old references). The very recent theoretical touch on the Poisson-Nernst-Planck equation was initiated by Bazant group [24–27]. They considered the induced-charge electroosmosis around a conducting circular cylinder and showed that various flow patterns are possible depending on the externally applied electric field. They then applied their analytical method to the transient charging of an electrolyte between a pair of facing electrodes caused by impulsive application of a constant potential difference between the electrodes [24]. Their important findings and the possible applications are summarized in [21]. They also conducted a simple experiment for the case with a metal wire located within a microchannel receiving ac field [25]. Their capacitor model, however, showed deviation from the experimental observation. On the contrary, the model of Green *et al.* [8] fitted the data well, but the physical ground of their model has not been established yet.

In this paper we propose the electrical triple layer (or electric quadruple layer when the transient is included) instead of the EDL as the correct structure of the electrokinetic thin layer near the electrode surface as far as the ion transport is concerned in a nonlinear regime under ac field. Our assertion is firstly based on the numerical solution to the one-dimensional (1D) Poisson-Nernst-Planck equation, and then it is verified from the asymptotic solutions for each layer. In the following section, we will present the governing equations and the numerical methods. The asymptotic analysis is then provided in Sec. III for each of the three layers. The approximate equations in each layer are derived in part from an order-estimation principle and in part from the numerical results. A simple dynamical equation for the surface charge density (charge per unit area), which can be used as a boundary condition for the Laplace equation for the potential in the bulk, is next derived. We apply our asymptotic method to the ion-transport problem within two parallel facing electrodes to validate our model. In this section, we also describe in detail the role of the middle layer in the ion-transport process through the whole layer. Further discussion on the issue of the multiple-layer structure of the nearby field of the electrodes is provided in Sec. VI. Effect of the ion adsorption at the interface between the Stern and inner layers on the ion transport is then discussed in Sec. VII with the aid of the asymptotic solutions, which is followed by conclusions in Sec. VII.

II. GOVERNING EQUATIONS AND NUMERICAL METHODS

Time evolution of the ion number concentrations c^{*+} and c^{*-}, the electric potential ϕ^* and the electric charge density (charge per unit volume) ρ_e^* is determined by the following Poisson-Nernst-Planck equations (see, e.g. [24]):

$$\frac{\partial c^{*\pm}}{\partial t^*} = D\left[\nabla^{*2}c^{*\pm} \pm \left(\frac{ze}{k_bT}\right)\nabla^* \cdot (c^{*\pm}\nabla^*\phi^*)\right], \tag{1a}$$

$$\nabla^* \cdot (\varepsilon\varepsilon_0\nabla^*\phi^*) = -\rho_e^*, \tag{1b}$$

$$\rho_e^* = (c^{*+} - c^{*-})ze, \tag{1c}$$

where t^* is the time, (x^*, y^*) the spatial coordinates for 2D problem, D the ion diffusivity, z the valence of the (symmetric) ions, e the electron charge, k_b the Boltzmann constant, T the temperature, ε the dielectric constant of the electrolyte, and ε_0 the permittivity of vacuum. In this formulation we assume a dilute monovalent symmetrical electrolyte ($z=1$) with uniform temperature so that D, ε and T remain constant. The first and second terms within brackets on the right-hand side (RHS) of Eq. (1a) reflect the diffusion and conduction (or migration) of ions, respectively. In order to make the equations dimensionless, the variables are scaled as follows:

$(x^*, y^*) = L(x,y)$, $t^* = t/\omega$, $c^{*\pm} = c_0^* c^{\pm}$, $\phi^* = \phi_{\text{ref}}^* \phi$, and $\rho_e^* = c_0^* ze\rho_e$, where L is the reference length such as distance between the electrodes, ω the angular frequency of the external ac potential, c_0^* the bulk concentration of each ion, and $\phi_{\text{ref}}^* = (L/\lambda_d)^2 (D/L^2\omega)\varsigma^*/2$ the reference potential. Selecting this as the reference potential is just a matter of convenience; the number of dimensionless parameters explicitly appearing in the dimensionless equations is reduced (but additional parameter of course appears in the boundary condition). Further, $\lambda_d = \sqrt{\varepsilon\varepsilon_0 k_b T/2c_0^* z^2 e^2}$ is the Debye screening length and $\varsigma^* = k_b T/ze$ the thermal potential. Then the dimensionless form of Eqs. (1a)–(1c) is

$$\frac{\partial c^{\pm}}{\partial t} = \varepsilon_1^2 [\nabla^2 c^{\pm} \pm \gamma \nabla \cdot (c^{\pm} \nabla \phi)], \tag{2a}$$

$$\varepsilon_1^2 \nabla^2 \phi = -\rho_e, \tag{2b}$$

$$\rho_e = (c^+ - c^-), \tag{2c}$$

where dimensionless parameters are

$$\gamma = \phi_{\text{ref}}^*/\varsigma^* = \frac{1}{2}(L/\lambda_d)^2 \varepsilon_1^2, \quad \varepsilon_1 = \sqrt{D/L^2\omega}. \tag{3}$$

In deriving Eq. (2b) from Eq. (1b), it is assumed that ε is constant. Interpretation of these parameters is easier if we introduce the diffusion length scale

$$\lambda_{\text{dif}} = \sqrt{D/\omega}, \tag{4}$$

that represents the spatial range in which diffusion of the ion concentrations takes place during the ac time scale $1/\omega$ (in fact, λ_{dif} corresponds to the middle-layer thickness as will be shown later). Then, ε_1 can be understood as the ratio of λ_{dif} to the bulk size L, i.e., $\varepsilon_1 = \lambda_{\text{dif}}/L$. Further, γ can be interpreted as either the ratio of the reference potential to the thermal potential, as explicitly shown in Eq. (3), or $\gamma = (\lambda_{\text{dif}}/\sqrt{2}\lambda_d)^2$ in terms of the length scales.

We expect a thin layer structure near the electrode and also the bulk region outside the layer. Ions are expected to be neutralized in the bulk region, and so the following Laplace equation governs the potential distribution in the bulk:

$$\nabla^2 \phi = 0. \tag{5}$$

For a typical example, we assume $L = 20\ \mu\text{m}$, $\omega = 100$ rad/s, $D = 10^{-10}\ \text{m}^2/\text{s}$, $T = 300$ K, and the bulk concentration 10^{-3} M of KCl solution. Then, we get $\varsigma^* = 26$ mV, $\varepsilon_1 = 0.05$, and $\gamma = 5260$. Notice that the value of γ is very large for this typical case. Here, we are interested in the case of small ε_1 and large γ so that the nonlinear, ion migration term can have the same importance as the diffusive term in the inner layer.

In this study, we further assume that the variation of the variables along the electrode surface is much smaller than that along the normal direction. Under this assumption, Eqs. (2a)–(2c) are simplified to 1D form as follows.

$$2\frac{\partial f}{\partial t} = \frac{\partial^2 f}{\partial Y^2} + \frac{\partial}{\partial Y}\left(\gamma f \frac{\partial \phi}{\partial Y}\right), \tag{6a}$$

$$2\frac{\partial g}{\partial t} = \frac{\partial^2 g}{\partial Y^2} - \frac{\partial}{\partial Y}\left(\gamma g \frac{\partial \phi}{\partial Y}\right), \tag{6b}$$

$$\frac{\partial^2 \phi}{\partial Y^2} = 2(g - f), \tag{6c}$$

where c^+ and c^- are replaced with f and g, respectively, and $Y = n/(\sqrt{2}\varepsilon_1)$ is used to strain the dimensionless normal coordinate $n = n^*/L$.

We need boundary conditions for f and g. In this study we do not consider electrode reaction, i.e., we assume completely polarized electrodes. Under this assumption, usually the zero ion-flux is applied at $Y = 0$, the outer edge of the Stern layer. However, we permit non-specific ion adsorption of ions at $Y = 0$ so that we have

$$\frac{d\Gamma^{\pm}}{dt} = J_0^{\pm}, \tag{7}$$

where $J_0^{\pm}$ denotes the dimensionless flux of each ion

$$J^{\pm} = \frac{\partial c^{\pm}}{\partial Y} \pm \gamma c^{\pm} \frac{\partial \phi}{\partial Y} \tag{8}$$

evaluated at $Y = 0$, and $\Gamma^{\pm}$ the dimensionless areal concentration of each ion adsorbed at the interface. We further need the relation between the adsorbed amount of ions and the nearby concentration of ions at the interface. In this study we employ the following formula:

$$\Gamma^+ = \frac{\Gamma_{\max} \alpha f_0}{1 + \alpha(f_0 + g_0)}, \tag{9a}$$

$$\Gamma^- = \frac{\Gamma_{\max} \alpha g_0}{1 + \alpha(f_0 + g_0)}, \tag{9b}$$

where f_0 and g_0 indicate evaluation of f and g at $Y = 0$. In fact, Eqs. (9a) and (9b) correspond to the Langmuir isotherm. Here $\Gamma_{\max}$ is the limit value of $\Gamma^{\pm}$ available at $f_0 \to \infty$ or $g_0 \to \infty$. Its physical value $\Gamma_{\max}^*$ should be of $O(1/a^{*2})$ where a^* is the ionic radius. Further, the dimensionless parameter α controls the rate of increase of $\Gamma^{\pm}$ upon change of f_0 or g_0 for their small values. It can be shown that the reference quantities for nondimensionalization are $J_{\text{ref}}^* = Dc_0^*/(\sqrt{2}\varepsilon_1 L)$ for $J^{\pm}$ and $\Gamma_{\text{ref}}^* = J_{\text{ref}}^*/\omega$ for $\Gamma^{\pm}$ and $\Gamma_{\max}$. We may use different values of $\Gamma_{\max}$ and α for cations and anions, but for the simplicity of formulation we take the same values for both. It should be noted that similar isotherm has been used by Mangelsdorf and White [28,29] in their linear analysis of the mobility of spherical colloidal particles under ac. In fact, we follow their assumption that the adsorption time scale is short enough so that equilibrium state of Eqs. (9a) and (9b) is readily attained between the adsorbed ions and nonadsorbed nearby ions.

Boundary condition for the potential at $Y = 0$ can be derived from the fact that the Stern layer has no charge accumulation ($\rho_e^* = 0$) but the interface has nonequilibrium adsorption ($\Gamma^+ \neq \Gamma^-$). Neglecting again the tangential variation of ϕ^*, we can derive from integration of Eq. (1b) the fact that the potential gradient within the Stern layer is uniform.

This gradient is readily formulated in terms of the electrode potential $V_0^* = V_{00}^* \cos \omega t^*$, the potential at the interface ϕ_0^* and the Stern-layer thickness λ_S as follows.

$$\left(\frac{\partial \phi^*}{\partial n^*}\right)_{0-} = \frac{\phi_0^* - V_{00}^* \cos \omega t^*}{\lambda_S}.$$

Here, V_{00}^* is the amplitude of the external ac potential. Next, we integrate Eq. (1b) over the infinitely thin interface, where adsorbed ions are accumulated, to get

$$\varepsilon \varepsilon_0 \left(\frac{\partial \phi^*}{\partial n^*}\right)_{0+} - \varepsilon_S \varepsilon_0 \left(\frac{\partial \phi^*}{\partial n^*}\right)_{0-} = -ze(\Gamma^{*+} - \Gamma^{*-}),$$

where ε_S denotes the dielectric constant of the Stern layer. Then, we obtain the following dimensionless equation:

$$\phi_0 = V_{00} \cos t + \varepsilon_2 \left(\frac{\partial \phi}{\partial Y}\right)_0 + \varepsilon_2 \sigma_a, \qquad (10)$$

where σ_a, the dimensionless surface charge density caused by the adsorption, is given by $\sigma_a = \Gamma^+ - \Gamma^-$, and

$$\varepsilon_2 = \frac{\lambda_S \varepsilon / \varepsilon_S}{\sqrt{2}\varepsilon_1 L}. \qquad (11)$$

The numerator in Eq. (11) can be considered as an effective thickness of the Stern layer; $\lambda_{\mathrm{Seff}} = \lambda_S \varepsilon / \varepsilon_S$. Then the small parameter ε_2 can be understood in terms of the length scales as $\varepsilon_2 = \lambda_{\mathrm{Seff}} / \sqrt{2} \lambda_{\mathrm{dif}}$.

As the boundary conditions for Eqs. (6a) and (6b) at the outer edge of the layer, we apply two kinds. When the bulk space is much larger than the layer, we simply assume that the bulk concentrations remain at the equilibrium values: $f = g = 1$ at $Y = Y_m$, where Y_m denotes the end of the computational domain. For the case of parallel facing electrodes with half spacing Y_m, to be presented in Sec. IV, we set the symmetric boundary condition: $\partial f / \partial Y = \partial g / \partial Y = 0$ at $Y = Y_m$. The boundary condition for Eq. (6c) at the outer edge of the layer depends on a specific problem in hand.

The numerical solutions of Eqs. (6a)–(6c) were obtained by using a finite volume method with very fine grids near $Y = 0$ to resolve very steep profile of the variables in this region. The grid refinement was established by setting uniform grids in a new variable η and using the following map function:

$$Y = Y_n{}' \eta + \frac{1}{2}(Y_p{}' - Y_n{}') \left[\eta + \frac{1}{s} \ln\left(\frac{\cosh s(\eta - \eta_e)}{\cosh s \eta_e} \right) \right],$$

where Y_n' and Y_p' are constants representing the relative size of the grid spacing at $Y = 0$ and $Y = Y_m$, respectively, and $\eta = \eta_e$ denotes the border between the fine-grid region for the inner layer and the coarse-grid region for the rest. The parameter s controls the spatial range of the grid variation near $\eta = \eta_e$. Those parameters are determined from several requirements. First we set $\eta_m = Y_m$. Then 10% of the total grids are designed to be clustered in the inner layer, i.e., we set $\eta_e = 0.1 \eta_m$, and the inner layer thickness is estimated to be $Y_e = 5 / \sqrt{\gamma}$ based on the asymptotic solution; at low L values, however, we increase η_e in order to avoid numerical instability. We also apply an empirical formula $Y_n{}' = 0.05(Y_e / \eta_e)$ based on several test runs. Typical values used in this study are $Y_m = \eta_m = 18$, $\eta_e = 1.8$, $Y_p{}' = 1.11$, $Y_n{}' = 0.0013$, and $s = 8.8$ for the total number of grids 4000. The variables f, g, and ϕ are defined at the same nodal points. The Crank-Nicolson method is applied in treating the transient term, and a fully implicit algorithm is applied in time advancing. Use of the implicit algorithm then permits us to choose a rather large time increment Δt, its typical value being 0.003.

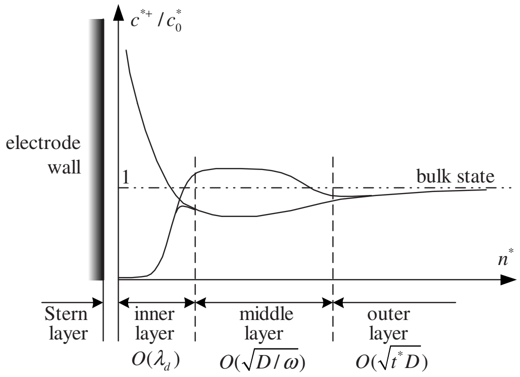

FIG. 1. Dynamical range of the cation's concentration during one period of ac. Note that the inner layer oscillates once and the middle layer twice per external period. The outer layer shows quasisteady dispersion of concentrations expanding to the bulk and finally disappears after a long time.

When one wants to perform numerical simulation of Eqs. (2a)–(2c) for the whole region of the electrolyte surrounding the electrodes, including both the bulk region and the thin layer, one may need to satisfy an enormous storage requirement because the thin layer must be resolved with very fine mesh and the bulk region, much wider than the layer, also needs considerable number of grids. More importantly, the system of equations must be solved in a transient way because the ion transport within the layer is highly nonlinear in most practical problems. In this case, the analytic form of the solutions for the ion transport problem as will be provided in the following section may reduce the computational requirement enormously.

III. ASYMPTOTIC SOLUTIONS

We present asymptotic solutions of the 1D equations (6a)–(6c). As stated previously, we are interested in the case of large γ, so that the governing equations are nonlinear. (Notice that Bazant *et al.* [24] defined the nonlinearity by the ratio λ_d / L.) It was found from many numerical simulations at large γ that there exist three subregions within the layer aside from the Stern layer, in each of which the solution takes distinctively different form, as illustrated in Fig. 1. The innermost region (to be called "inner layer" hereafter) is the thinnest and is characterized by a very steep spatial profile of variables evolving in time with the same fundamental frequency as the external one, in a nonlinear (nonharmonic) manner. The region next to the inner layer (to be called "middle layer") is thicker than the inner layer, but the variables change more smoothly in time with the frequency twice that of the external one. The outermost layer (to be called "outer layer") shows quasisteady development of the variables and the region expands slowly in time, in a really diffusive manner. Such distinctive nature of the solutions in each layer of course comes from the fact that each term in Eqs. (6a) and (6b) shows a completely different level of relative importance depending on the layer. Within the inner layer, the numerical results show that the LHS terms of Eqs. (6a) and (6b) are negligibly small and the diffusion and conduction terms balance with each other. Within the middle and outer layers, the conduction term is negligible and the transient and diffusion terms balance with each other.

A. Inner layer

Based on our numerical results, we expect a very thin inner layer near $Y=0$, its thickness being observed to decrease as γ is increased. So, we may put $Y\sim\gamma^{-n}$, $\phi/f\sim\gamma^{-m}$ and $g/f\sim 1$ $(m,n>0)$, estimate the order of magnitude of each term in Eqs. (6a)–(6c) and consider the balance of magnitude among those terms to derive $m=1$ and $n=1/2$. In the limit of $\gamma\to\infty$, therefore, we can neglect the LHS of Eqs. (6a) and (6b), which is in accordance with the numerical results. Finally, we propose the following form of approximate equations for the inner layer:

$$f' + \gamma f\Phi = 0, \tag{12a}$$

$$g' - \gamma g\Phi = 0, \tag{12b}$$

where $\Phi=\partial\phi/\partial Y$ is the potential gradient and the prime denotes $\partial/\partial Y$. These results just indicate that the charging time in the inner layer is much shorter than the external forcing period; i.e., the quasiequilibrium assumption holds in this layer (see, e.g. [24]). These equations are to be solved together with Eq. (6c). For the moment, we derive the Boltzmann distribution equations: $f=\exp[-\gamma(\phi-\phi_\infty)]$ and $g=\exp[+\gamma(\phi-\phi_\infty)]$, where ϕ_∞ stands for the asymptotic value of ϕ at infinity. Hereinafter the subscript ∞ indicates the asymptotic value of the variable at infinity, $Y\to\infty$, i.e., the outer limit of the inner variable.

To obtain the analytic solutions for the inner layer equations, we first multiply Eq. (6c) by Φ, apply Eqs. (12a) and (12b), and then integrate once to get

$$f + g = \frac{\gamma}{4}\Phi^2 + 2, \tag{13}$$

where Φ_∞ has been neglected. Subtracting Eq. (12b) from Eq. (12a) and substituting Eqs. (13) and (6c) into the result yields

$$\Phi'' = \gamma\Phi\left(\frac{\gamma}{2}\Phi^2 + 4\right).$$

Multiply this by Φ' and integrate once more to obtain

$$\Phi' = -\Phi\sqrt{\frac{\gamma^2}{4}\Phi^2 + 4\gamma}.$$

The negative sign was chosen to ensure $\Phi\to 0$ as $Y\to\infty$. This is integrated to become

$$\Phi = \frac{\pm\sqrt{16/\gamma}}{\sinh[\sqrt{4\gamma}(Y+Y_0)]}, \tag{14}$$

where the integration constant $Y_0(t)$ should be determined from an integral constraint to be satisfied over the whole layer. Explanation will be given shortly as to which sign should be chosen in Eq. (14). We can integrate this once more to obtain ϕ:

$$\phi = \phi_\infty \pm \frac{1}{\gamma}\ln\left|\frac{\cosh[\sqrt{4\gamma}(Y+Y_0)]-1}{\cosh[\sqrt{4\gamma}(Y+Y_0)]+1}\right|. \tag{15}$$

The solution f can be obtained by substituting Eq. (14) into Eq. (12a) and integrating the result:

$$f = \left[\frac{\cosh[\sqrt{4\gamma}(Y+Y_0)]+1}{\cosh[\sqrt{4\gamma}(Y+Y_0)]-1}\right]^{\pm 1}. \tag{16}$$

The anion's concentration g is the inverse of f in this layer, that is $g=f^{-1}$. By introducing a new variable $q(t)$ defined as the Φ value evaluated at $Y=0$, we can write f and ϕ in terms of q instead of Y_0 as follows:

$$f = \frac{\sqrt{16/\gamma+q^2}\cosh(\sqrt{4\gamma}Y) + \sqrt{16/\gamma}\sinh(\sqrt{4\gamma}Y) + q}{\sqrt{16/\gamma+q^2}\cosh(\sqrt{4\gamma}Y) + \sqrt{16/\gamma}\sinh(\sqrt{4\gamma}Y) - q}, \tag{17}$$

$$\phi = \phi_\infty - \frac{1}{\gamma}\ln f. \tag{18}$$

The relation between q and Y_0 can be derived by evaluating Eq. (14) at $Y=0$:

$$q = \frac{\pm\sqrt{16/\gamma}}{\sinh(\sqrt{4\gamma}Y_0)}. \tag{19}$$

It can be shown that q corresponds to dimensionless areal charge density caused by the nonequilibrium distribution of ions in the inner layer. In order to avoid singularity at $Y=Y_0$ [refer to Eq. (14)], we must ensure $Y_0>0$. This means we must choose the +sign for $q>0$ and the −sign for $q<0$. In fact, the solutions derived so far are known as the Gouy-Chapman-Stern model [24].

Now to obtain the equation that determines the function $q(t)$ or $Y_0(t)$, we use the integral constraint

$$2\int_0^\infty \frac{\partial(f-g)}{\partial t}dY = 2\gamma\Phi_\infty - (J_0^+ - J_0^-), \tag{20}$$

which can be derived by subtracting Eq. (6b) from Eq. (6a), integrating over the full domain, and then applying the boundary conditions (7). As will be shown later, the integrand on the LHS of Eq. (20) vanishes in the middle and outer layers because $f=g$ asymptotically in these layers. Therefore, it suffices to consider only the inner layer solutions in evaluation of the LHS term of Eq. (20); but this simplification does not hold for the integral constraint for each of f and g, because the middle layer contains the comparable amount of ions as will be shown in the middle-layer analysis. The LHS of Eq. (20) becomes $(g_0-f_0)dY_0/dt$. We can derive the formula for dY_0/dt in terms of dq/dt from Eq. (19) and that for g_0-f_0 or $f_0^{-1}-f_0$ from Eq. (17). Then LHS of Eq. (20) simply becomes dq/dt. On the other hand, the second term on the RHS of Eq. (20) can be shown after some algebra to become

$$J_0^+ - J_0^- = \beta\frac{dq}{dt},$$

where β is a function of q:

$$\beta = \frac{8\Gamma_{\max}\alpha\sqrt{\gamma}(8+16\alpha+\gamma q^2)}{\sqrt{16+\gamma q^2}(4+8\alpha+\alpha\gamma q^2)}. \tag{21}$$

Then Eq. (20) reduces to

$$\frac{dq}{dt} = \frac{2\gamma\Phi_\infty}{1+\beta}. \tag{22}$$

This very simple dynamic equation indicates that the function $q(t)$ is determined from the potential gradient, or the normal component of the electric field, at infinity and the factor $\beta > 0$ representing the adsorption effect. Further, we note that inclusion of the adsorption brings decrease of the magnitude of the areal charge density q within the inner layer for the same external potential gradient Φ_∞.

We now consider the Stern layer model (10). The LHS term ϕ_0 can be written in terms of q from Eqs. (17) and (18) as follows:

$$\phi_0 = \phi_\infty + \frac{1}{\gamma}\ln\left|\frac{\sqrt{16/\gamma+q^2}-q}{\sqrt{16/\gamma+q^2}+q}\right|. \tag{23}$$

Then Eq. (10) becomes

$$\phi_\infty = V_{00}\cos t + \varepsilon_2 q - \frac{1}{\gamma}\ln\left(\frac{\sqrt{16/\gamma+q^2}-q}{\sqrt{16/\gamma+q^2}+q}\right) + \varepsilon_2\sigma_a, \tag{24}$$

where σ_a is explicitly calculated from

$$\sigma_a = \frac{\Gamma_{\max}\alpha\gamma q\sqrt{16/\gamma+q^2}}{4+8\alpha+\alpha\gamma q^2}. \tag{25}$$

Now, the results obtained so far clearly demonstrate how the interaction between the inner layer and the bulk can be implemented. First, Eq. (22) is used to calculate q. Next, f_0 and g_0 are determined from Eq. (17) with $Y=0$ and $g_0=f_0^{-1}$. Then, $\Gamma^\pm$ is given from Eqs. (9a) and (9b). Equation (24) is next used to determine ϕ_∞, which then serves as one of the boundary conditions on the electrode surface when solving the bulk equation (5). The solution of Eq. (5) finally supplies the potential gradient Φ_∞, which is again used in calculating q from Eq. (22), where β is calculated by using Eq. (21). This completes one cycle of the single time-step computation, and the computation continues until a periodic state is reached.

For later use in the middle-layer analysis, we analyze a symmetric property of the function $q(t)$. Replacing $q \to -q$, $t \to t-\pi$ and $\phi \to -\phi$ in Eqs. (22) and (24) makes the equations invariant. This means that when $q(t)$ is expanded in Fourier series, all the even modes vanish and only the odd modes remain, and this was also confirmed from the numerical results.

B. Middle layer

Based on the numerical results, we propose the following approximate equation for f in the middle layer:

$$2\frac{\partial f}{\partial t} = \frac{\partial^2 f}{\partial Y^2}. \tag{26}$$

This can be derived under the assumptions that within the middle layer the net charge is zero, or $f=g$, and

$$\frac{\varepsilon_1 V_{00}^*}{\varsigma^*} \ll 1. \tag{27}$$

Balance between the transient and diffusion term, i.e., Eq. (26), means that the thickness of the middle layer should be of $O(\lambda_{\mathrm{dif}})$, where the diffusion length scale λ_{dif} is defined as Eq. (4).

It suffices to show derivation of the solution f because the governing equation and the relevant boundary conditions for g are identical with those for f. The solution of Eq. (26) can be written in a series form as follows:

$$f = f_\infty + \sum_{n=2,4,\ldots}^{\infty} \exp(-\sqrt{n}Y)[a_n\cos(nt-\sqrt{n}Y) - b_n\sin(nt-\sqrt{n}Y)], \tag{28}$$

where $f_\infty(t)$ is a slowly varying function of time to be determined from matching with the outer-layer solution. The constants a_n and b_n are determined from the integral constraint for f over the whole domain:

$$\int_0^\infty \frac{\partial f}{\partial t}dY = \frac{1}{2}\gamma\Phi_\infty - \frac{1}{2}J_0^+ = \frac{1}{4}\frac{dq}{dt} - \frac{1}{4}\left(\frac{d\Gamma^+}{dt} + \frac{d\Gamma^-}{dt}\right). \tag{29}$$

In evaluating the LHS we must consider not only the middle layer but also the inner-layer and outer-layer solutions. Fortunately, however, the outer layer is characterized by a quasisteady solution as will be shown shortly. Since the unknown constants in Eq. (28) are to be determined from the oscillatory components of the solution, we do not have to consider the outer-layer solution in this analysis. Suppose now the concentration f is composed of the inner-layer and middle-layer contributions: $f=f_{\mathrm{i}}+f_{\mathrm{m}}-1$. Substituting this into LHS of Eq. (29) and applying the formula for the inner-layer solution f_{i} obtained so far results in

$$-4\int_0^\infty \frac{\partial f_m}{\partial t}dY = \left[\frac{1}{\sqrt{16/\gamma+q^2}} + \frac{8\Gamma_\infty\alpha\gamma}{(4+8\alpha+\alpha\gamma q^2)^2}\right]q\frac{dq}{dt}, \tag{30}$$

where the term representing the contribution of the adsorption is deduced from Eqs. (9a) and (9b) together with Eq. (17) evaluated at $Y=0$ and $g_0=f_0^{-1}$.

Now, we can expand the RHS of Eq. (30) in a Fourier series:

$$\text{RHS of Eq. (30)} = \sum_{n=2,4,\ldots}^{\infty} (c_n \cos nt + d_n \sin nt).$$

The reason for considering only the even modes can be understood from the fact that, as shown in the proceeding section, the function q is composed of the odd modes only. Then we substitute Eq. (28) into the LHS of Eq. (30) and, after integration, equate the same mode to obtain

$$a_n = \frac{d_n - c_n}{4\sqrt{n}}, \quad b_n = \frac{d_n + c_n}{4\sqrt{n}} \quad (n = 2,4, \ldots). \tag{31}$$

Note, in addition, that $\Phi' = 0$ in the middle layer because $f = g$; this means that the potential profile should be linear in the middle layer. We can also predict a peculiar behavior of the concentrations in this layer. Since the odd mode is vanishing in Eq. (28), the fundamental mode is of second harmonic; in more practical terms, the concentration should oscillate in time at a frequency twice that of the external one. The reason for such peculiar behavior will be further discussed in physical terms in the next section.

C. Outer layer

In the outer layer the appropriate equation for f takes the same form as that in the inner layer, i.e., Eq. (26). Therefore in this layer, too, we derive $f = g$. The numerical solution implies that this layer is characterized by slowly varying functions of time. Therefore, we seek the solution of Eq. (26) in the following form:

$$f = 1 - C\frac{1}{\sqrt{2t}} \exp(-Y^2/2t), \tag{32}$$

where the unknown constant C is to be determined from the steady or quasisteady (hereafter to be called simply "quasisteady") part of the integral constraint (29); recall that in the analysis of the middle layer we have already satisfied the oscillatory part of Eq. (29). Let us decompose the function f in each layer into the oscillatory part $\tilde{f}$ and the quasisteady part $\bar{f}$, i.e., $f = \tilde{f} + \bar{f}$. Then the quasisteady part of the constraint (29) reads

$$\frac{\partial}{\partial t}\int_0^{\infty} (\bar{f}_i + \bar{f}_{\mathrm{m}} + \bar{f}_{\mathrm{o}} - 2 - f_{\infty}) dY = 0.$$

Initially, $f = 1$ is imposed everywhere. Therefore, this constraint is equivalent to

$$\int_0^{\infty} (\bar{f}_{\mathrm{o}} - 1) dY + \int_0^{\infty} (\bar{f}_i - 1) dY = 0, \tag{33}$$

where $\bar{f}_{\mathrm{m}} = f_{\infty}$ is used. We can integrate the first term of Eq. (33) by applying Eq. (32) and the second term by Eq. (17) to obtain

$$C = \frac{1}{2\sqrt{\pi}}\left(\frac{1}{2\pi}\int_0^{2\pi} \sqrt{16/\gamma + q^2} dt - \sqrt{16/\gamma}\right). \tag{34}$$

Matching with the middle layer further provides the formula for $f_{\infty}(t)$:

$$f_{\infty} = 1 - \frac{C}{\sqrt{2t}}. \tag{35}$$

When the initial distribution of f (and g) is intentionally given such that the non-zero value of $f - 1$ (and $g - 1$) occurs only in the inner layer and the integral of this is the same as the second term of Eq. (33), then the value C should be almost zero.

The composite solution for the concentration is constructed by summing up all the contributions from the three layers and then subtracting the common parts:

$$f = f_i + f_{\mathrm{m}} + f_{\mathrm{o}} - f_{\infty} - 1,$$

which applies to the anion concentration too. On the other hand, the net electric potential is given by summing the potential in the inner layer ϕ_i and that in the bulk ϕ_b and then by subtracting the common value:

$$\phi = \phi_i + \phi_b - \phi_{\infty}$$

IV. VALIDATION OF THE SOLUTIONS

In order to validate our asymptotic solutions, we consider the ion transport problem in a cell confined between two parallel facing electrodes. We assume an infinite extent of the electrodes so that 1D analysis became valid for both the layer and the bulk. The distance between one of the electrodes and the centerline is chosen as the length scale L. Let one of the electrodes be situated at $Y = 0$ and the centerline at $Y = Y_m$. Then the potential in the bulk has the linear profile

$$\phi = \phi_{\infty} - \left(\frac{\phi_{\infty}}{Y_m}\right) Y,$$

where ϕ_{∞}, to be determined from Eq. (24), corresponds to the bulk potential evaluated on the electrode surface. Applying this to Eq. (22) and using Eq. (24), we obtain the following dynamical equation for q:

$$\frac{dq}{dt} = \frac{2}{(1+\beta)Y_m}\left[\ln\left(\frac{\sqrt{16/\gamma + q^2} - q}{\sqrt{16/\gamma + q^2} + q}\right) - \varepsilon_2 \gamma q - \gamma V_{00} \cos t - \varepsilon_2 \sigma_a\right]. \tag{36}$$

From the numerical simulation of this, we have found that after a few periods the solution q approaches to a periodic state regardless of the initial value for q. Notice that the RHS can be evaluated explicitly and thus it is not required to solve a nonlinear algebraic equation as in the dynamical equation proposed by Bazant *et al.* [24]. Further, their solution is given in an integral form, but in a practical sense the two solutions should be equivalent except for the adsorption terms, of course.

As a typical case, we set $L = 100$ μm and choose "electrolyte A" of HCl used in Refs. [5,8]: $c_0^* = c_{0A}^* \equiv 0.85 \times 10^{23}$ m^{-3}; $D = 1.92 \times 10^{-9}$ m^2/s. Further, we assume $T = 288$ K, $\lambda_{\mathrm{Seff}} = 3.5$ nm, $V_{00}^* = 0.25$ V, and set the frequency of the applied potential at 100 Hz. This set of the parameter

TABLE I. Coefficients a_n and b_n used in the middle-layer solution (28) obtained from Eq. (31) and Fourier expansion of the RHS of Eq. (30).

n	a_n	b_n
2	-0.374×10^{-1}	0.644×10^{-1}
4	-0.130×10^{-1}	-0.867×10^{-2}
6	0.293×10^{-2}	-0.526×10^{-2}
8	0.254×10^{-2}	0.109×10^{-2}
10	-0.398×10^{-3}	0.133×10^{-2}
12	-0.721×10^{-3}	-0.127×10^{-3}
14	0.222×10^{-4}	-0.400×10^{-3}

values will be referred to as "standard" hereinafter. Then we get $\varsigma^*=24.8$ mV, $\lambda_d=25.4$ nm, $\varepsilon_1=0.017$, $\varepsilon_2=0.00142$, $V_{00}=0.00426$, and $\gamma=2363$. In addition, we do not consider the ion adsorption in this section for the understanding of the fundamental structure of the solutions; the adsorption effect will be addressed separately in the next section. The sequence of obtaining the asymptotic solution is simple. First, we obtain the time evolution of q from Eq. (36) with initial value $q=0$ and ϕ_∞ from Eq. (24) for 20 periods. From this we can compute the profiles of the inner layer solutions f and ϕ by using Eqs. (17) and (18), respectively. The data of the RHS of Eq. (30) taken during the final period of the calculation are then expanded in a Fourier series to produce the coefficients c_n and d_n, after which we compute the constants a_n and b_n from Eq. (31); Table I shows the first seven pairs of these constants. Further, the constant C is computed from Eq. (34) and $f_\infty(t)$ from Eq. (35); in this sample case, $C=0.0514$ and $f_\infty(t)=0.9967$ at $t=19.5T$, where $T=2\pi$ represents one period of the external ac in the dimensionless unit. These are next applied to Eq. (28) to obtain f in the middle layer and to Eq. (32) to obtain f in the outer layer.

Figure 2 shows the asymptotic solutions obtained in this way in comparison with the numerical ones obtained for the original equations (6a)–(6c) with the method described in the last part of Sec. II. In all the three layers the comparison shows excellent agreement between the numerical and asymptotic solutions. In the inner layer very steep increase of the concentrations is observed [Fig. 2(a)]. It also reveals increase of maximum of f_0 90 times as much as the bulk concentration. f_0 is further increased at higher γ and V_{00}. For instance, at the external potential of 2.5 V, that is 10 times the present setup, the asymptotic solution shows maximum of f_0 as much as 13 500. It is confirmed that the behavior of g is exactly inverse of f. Notice also that the concentrations in the inner layer show positive steady components for both

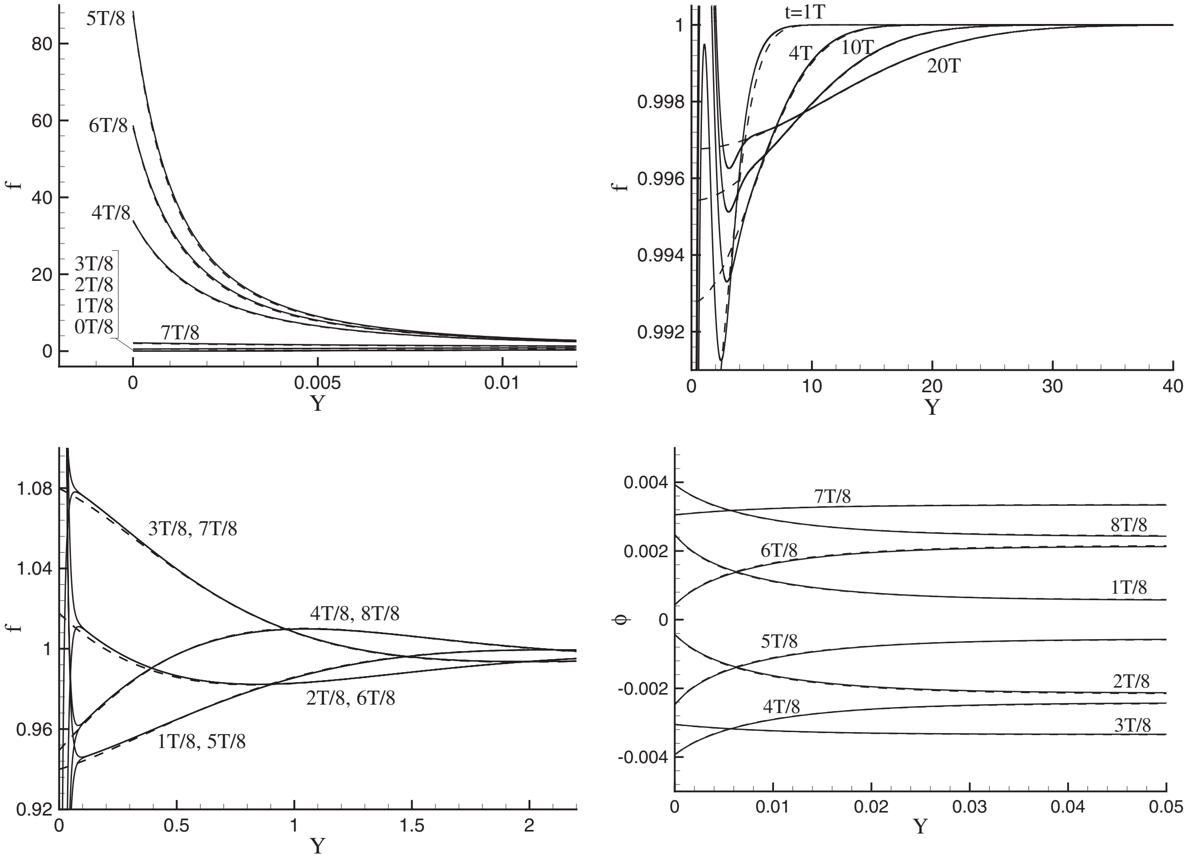

FIG. 2. Time evolution of profiles of the concentration f and potential ϕ obtained from the numerical simulation (solid lines) and asymptotic analysis (dashed lines) at the standard parameter set: (a) f in the inner layer during the 20th period; (b) f in the middle layer during the 20th period; (c) f in the outer layer at four instants; (d) ϕ in the inner layer during the 20th period. Notice that the middle-layer solution is constructed from the first three pairs of constants shown in Table I.

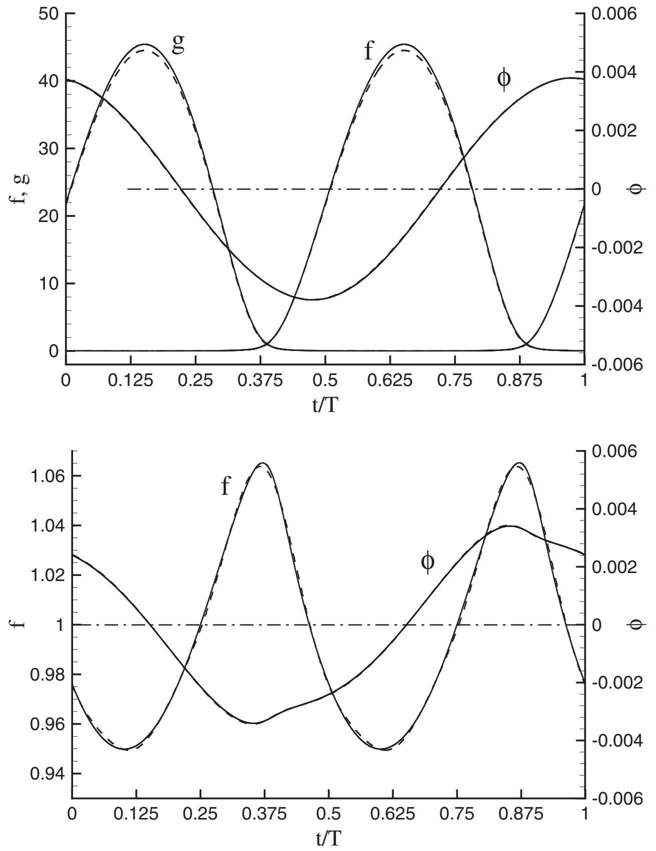

FIG. 3. Time evolution of the concentrations f and g and the potential ϕ obtained from the numerical simulation (solid lines) and asymptotic analysis (dashed lines) evaluated (a) at $Y=9.44\times10^{-4}$ (inner layer) and (b) at $Y=0.2256$ (middle layer) with the standard parameter set. The concentration g is not shown in (b) because it is indistinguishable from f.

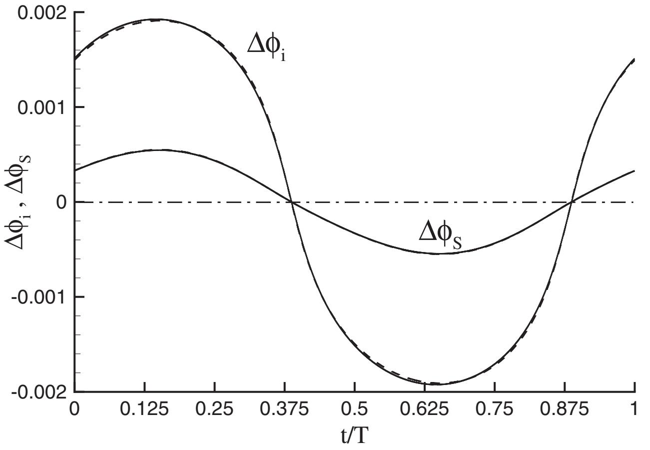

FIG. 4. Time evolution of the potential drop across the Stern layer $\Delta\phi_{\mathrm{S}}$ and that across the inner layer $\Delta\phi_{\mathrm{i}}$ obtained from the numerical simulation (solid lines) and asymptotic analysis (dashed lines) at the standard parameter set.

f and g, which necessitates the outer layer's quasisteady development in order to satisfy the mass conservation as will be discussed in more detail below. In the middle layer [Fig. 2(b)], the concentration oscillates in time with the frequency double that of the external one in accordance with the prediction presented in the previous analysis. Although variation of f remains much smaller than that in the inner layer, the spatial range of the middle layer where f varies is much larger than that of the inner layer. Figure 2(b) also reveals a distinctive border between the inner and middle layers at $Y=0.1$. In the outer layer $Y>2$ [Fig. 2(c)], the agreement between the numerical and asymptotic solutions for the quasisteady behavior is also excellent. This layer slowly expands in time and eventually will reach the centerline at $Y_m=40.5$; after this the asymptotic outer layer solution of course becomes less accurate [24]. The reason why the concentrations remain always less than 1 in this layer comes from the principle of mass (ionic concentration) conservation; in the inner layer the time average of concentrations is larger than 1, and so the outer layer must show the concentrations lower than 1. Time evolution of the potential profile, as shown in Fig. 2(d), indicates that the potential drop occurs only in the inner layer, as pointed out above [recall that outer edge of the inner layer is at $Y=0.1$; see Fig. 2(b)]. Also note that the potential drop is very gradual compared with those of the concentrations [compare Fig. 2(a) and 2(d)].

Figure 3 shows the time evolution of variables at a point chosen in the inner layer [Fig. 3(a)] and that in the middle layer [Fig. 3(b)]. In the inner layer the concentrations behave in nonharmonic (or nonlinear) manner and their time-average magnitudes are positive. On the other hand, the potential in this layer exhibits almost harmonic behavior. All the variables in this layer oscillate once per external-oscillation period. In the middle layer, the concentrations oscillate twice per period [Fig. 3(b)]. On the other hand, the potential shows single oscillation but the behavior is nonharmonic.

The mathematical reason for such double-frequency oscillation of the concentrations in the middle layer was given in Sec. III B. Here we try to understand that reason and the role of the middle layer by addressing the dynamics of the ion transport occurring across the three layers in physical terms. First we note that the potential drop across the Stern layer, $\Delta\phi_{\mathrm{S}}\equiv V_0-\phi_0$, is small as shown in Fig. 4, and thus the evolution of ϕ in the inner layer is not so different from that of the external potential as shown in Fig. 3(a). However, the potential drop across the inner layer $\Delta\phi_i\equiv\phi_0-\phi_\infty$ (Fig. 4) is significant, causes a decrease in the amplitude of the potential ϕ_∞ [almost the same as ϕ in the middle layer shown in Fig. 3(b)], and makes the phase of ϕ_∞ ahead of $V_0(t)$ as much as $T/8$; that is, $\Delta\phi_i$ is positive for $t/T=-1/8\sim3/8$ and negative for the other time interval during one period as shown in Fig. 4. Next we note that when ϕ_∞ is positive, the potential gradient at infinity Φ_∞ is negative, and vice versa. So, we understand that $\Phi_\infty>0$ for $t/T=2/8\sim5/8$ and $\Phi_\infty<0$ for the other interval. Our analysis is based on the above two underlying observations regarding time evolution of $\Delta\phi_i$ and Φ_∞. Further, we need to introduce integrated concentrations $F(t)$ and $G(t)$, the total amounts of fluctuating components of f and g per unit area, respectively, defined as

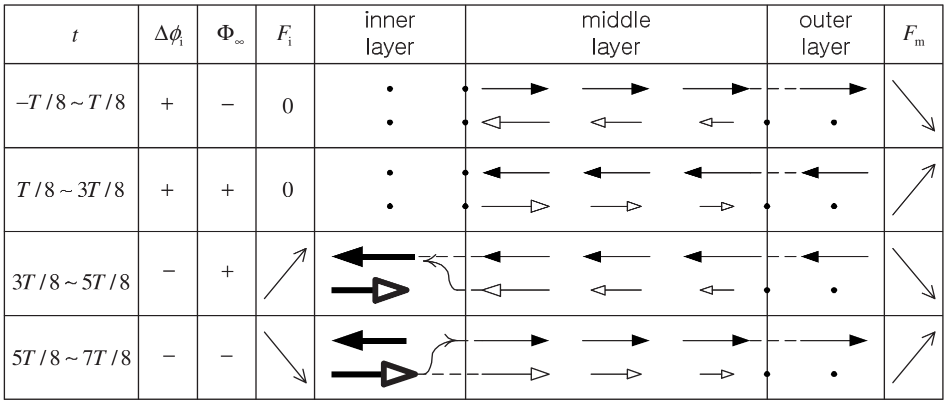

FIG. 5. Schematic illustrating the cation flux (horizontal arrows) in each of three layers and time change of the integrated cation-concentrations (inclined arrows) F_i and F_m. The filled arrowheads denote the conduction (or migration) flux whereas the open arrowheads the diffusion flux. The dashed lines across interfaces indicate the crossover of the flux and the solid dots zero flux.

$$F(t)=\int_0^\infty (f-\bar{f})dY,\quad G(t)=\int_0^\infty (g-\bar{g})dY.$$

Then, from Eq. (29) we obtain the rate of time change of these quantities, for the case without ion adsorption, as follows:

$$\dot{F}=\frac{1}{2}\gamma\Phi_\infty,\quad \dot{G}=-\frac{1}{2}\gamma\Phi_\infty. \tag{37}$$

On the other hand, F and G are composed of contributions from the inner and middle layers: $F=F_i+F_m$, $G=G_i+G_m$. The integrand in LHS of Eq. (20) is zero outside the inner layer, and thus

$$\dot{F}_i-\dot{G}_i=\gamma\Phi_\infty. \tag{38}$$

Then we can estimate the magnitudes of $\dot{F}_i$, $\dot{G}_i$, $\dot{F}_m$, and $\dot{G}_m$ from Eqs. (37) and (38). For the interval $t/T=-1/8\sim 3/8$, $\Delta\phi_i$ is positive and the Boltzmann distribution predicts $\dot{F}_i=0$. Therefore, we can derive $\dot{G}_i=-\gamma\Phi_\infty$ from Eq. (38). Further, from Eq. (37) we can derive $\dot{F}_m=\dot{G}_m=\gamma\Phi_\infty/2$. In this way, for the other interval $t/T=3/8-7/8$ we can predict the following: $\dot{F}_i=\gamma\Phi_\infty$, $\dot{G}_i=0$, and $\dot{F}_m=\dot{G}_m=-\gamma\Phi_\infty/2$. Here, we concentrate on the development of cations only, as shown in Fig. 5. In addition, we need to define the cation's concentration flux $J=-J^+$, where the current flux J^+ is defined in Eq. (8). Note $J_\infty=-\gamma\Phi_\infty$, where J_∞ stands for the flux at infinity (or in the outer layer). We also need to define the diffusion flux $J_d=-\partial f/\partial Y$ and the conduction flux $J_c=-\gamma f\Phi$, both contributing to the total flux, $J=J_d+J_c$; note that $J_d\cong 0$ in the outer layer, J_c is almost uniform over the middle and outer layers, and $J_d\cong -J_c$ in the inner layer although their magnitudes are very large.

Now we can address the dynamics of the ion transport. First we consider the time interval $t/T=-1/8\sim 1/8$. Since $\Phi_\infty<0$ in this interval, the flux J_∞ is positive, and the conduction flux J_c in the middle and outer layers also has the same magnitude as this. So, J_c is uniform in the middle layer as shown by the three arrows with identical lengths and solid heads in the middle-layer column on the first row in Fig. 5. On the other hand, in the inner layer f_i has already been decreased to zero, and so no cations are available, implying that the flux is zero at the interface between the inner and middle layers. Therefore for this time interval, crossover of the cations from the middle to the outer layer through the conduction flux is the only transport phenomenon, which results in the decrease of F_m as indicated by an inclined arrow in the last column on the first row of Fig. 5. Considering that f_m evaluated at $Y=0$ is roughly proportional to F_m, we can see that f_m near $Y=0$ must decrease during this time interval until it reaches a local minimum at $t/T=1/8$ as shown in Fig. 3(b); note that data shown in Fig. 3(b) are taken at $Y=0.2256$ which is very close to the interface between the inner and middle layers. For $t/T=1/8\sim 3/8$, $\Delta\phi_i$ is still positive and F_i remains at zero, but $\Phi_\infty>0$ and therefore the flux direction is reversed. This then results in the increase of F_m (see Fig. 5). Thus f_m increases until reaching maximum at the end of the interval $t/T=3/8$ as shown in Fig. 3(b). For $t/T=3/8\sim 5/8$, $\Delta\phi_i$ is now negative and so F_i is ready to increase. In this time interval we still have $\Phi_\infty>0$ and the bulk continues to supply positive charges to the middle layer but at the same time the inner layer now demands a larger amount of positive charges (almost double the amount supplied from the bulk to the middle layer; recall that $\dot{F}_i=\gamma\Phi_\infty$ and $\dot{F}_m=-\gamma\Phi_\infty/2$ as predicted previously). The middle layer provides the inner layer with the required flux $\gamma\Phi_\infty$, half by the diffusion and half by the conduction. So, the net effect is that the middle layer loses positive charges at the rate $\gamma\Phi_\infty/2$, resulting in the decrease of f_m until reaching minimum at $t/T=5/8$. Notice that during this interval, the fluxes in the inner layer are much larger than those in the other layers, and J_c is almost the same as $-J_d$. However, the former is slightly larger than the latter, as indicated by different lengths of arrows in Fig. 5, which contributes to the increase of F_i. For $t/T=5/8-7/8$, we have $\Phi_\infty<0$ and the bulk takes the positive charges away from the middle layer by conduction, and at the same time the inner layer pushes the charges into the middle layer with double the amount taken away by the bulk. The net effect is that f_m increases until it reaches a local maximum at $t/T=7/8$. A similar explanation can be made concerning the dynamics of anion concentration to show that its behavior is the same as that of the cation in the middle layer. The scenario described so far is enough to prove that the middle layer should show a double-frequency oscillation. Further, we have found the way in which it responds to the inner and outer layers' demand and supply of ions during one complete cycle of ac.

Next, we present the accuracy of the asymptotic solutions referring to the numerical ones for the full equations. For the analysis we define the rms error

$$\varepsilon_{\mathrm{rms}} = \frac{1}{\sqrt{\pi Y_{em}}V_{00}} \left\{ \int_0^{2\pi} \int_0^{Y_{em}} (\phi_{\mathrm{num}} - \phi_{\mathrm{asy}})^2 dY\, dt \right\}^{1/2},$$

where the spatial integration is performed over the distance twice the inner-layer thickness: $Y_{em}=2Y_e$. We investigated the effects of the half cell spacing L, the external frequency f_{req}, concentration c_0^*, and amplitude of the external potential V_{00}^* on the accuracy. Since we are interested in estimation of the accuracy of the asymptotic solutions for the practical cases, we present the results in terms of the dimensional parameters.

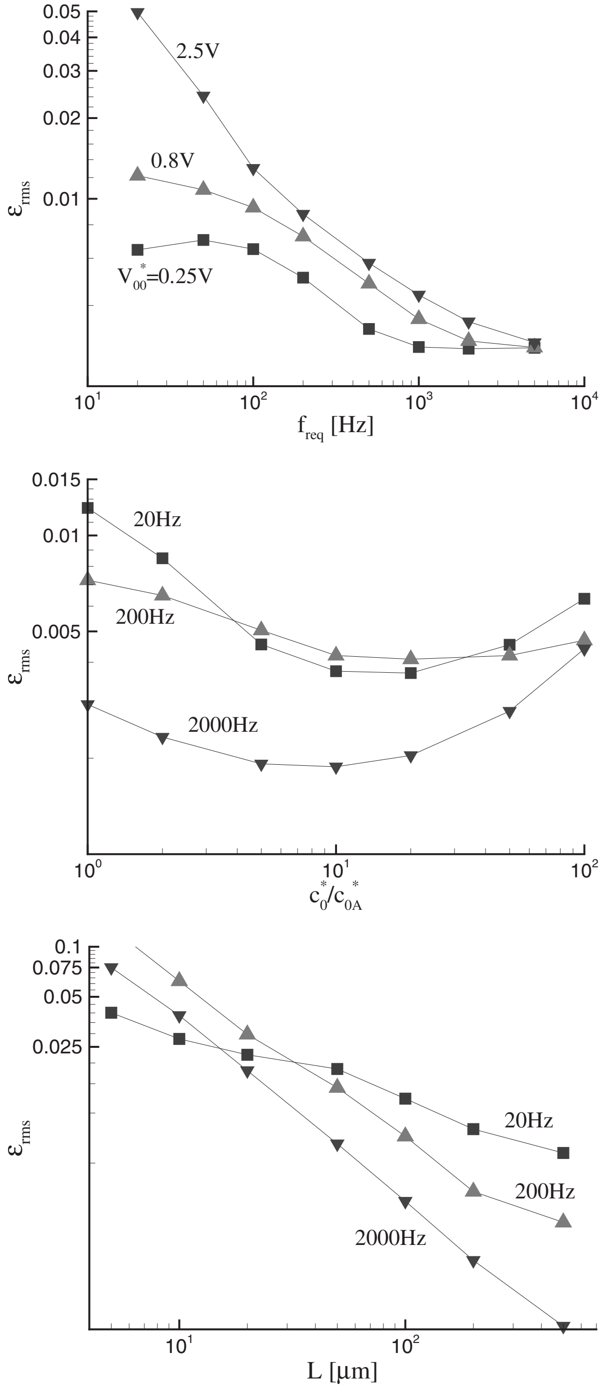

FIG. 6. rms error of the asymptotic solutions based on the numerical solutions: (a) $\varepsilon_{\mathrm{rms}}$ vs the frequency for three external potential values at $L=100$ μm and $c_0^*=c_{0A}^*$; (b) $\varepsilon_{\mathrm{rms}}$ vs the concentration ratio for three frequency values at at $L=100$ μm and $V_{00}^*=0.8$ V; (c) $\varepsilon_{\mathrm{rms}}$ vs the reference length L for three frequency values at $c_0^*=c_{0A}^*$ and $V_{00}^*=0.8$ V.

Figure 6 shows the dependence of $\varepsilon_{\mathrm{rms}}$ on f_{req}, c_0^* and L. It is seen that the errors overall remain at a low level, at most 13% for the case of the smallest spacing, $L=5$[μm]. At low external potentials, the error is not so much dependent on f_{req}; at high potentials, however, $\varepsilon_{\mathrm{rms}}$ increases significantly as f_{req} decreases [Fig. 6(a)]. Nor is $\varepsilon_{\mathrm{rms}}$ sensitive to the concentration change as shown in Fig. 6(b). The most significant influence comes from the change of L and the effect is more pronounced at high values of f_{req} than at low ones, as seen from Fig. 6(c). This figure indicates that at f_{req} higher than 200 Hz, $\varepsilon_{\mathrm{rms}}$ increases considerably as L decreases. The reason for such error increase at low L is attributed to the large fluctuation of the middle-layer concentrations caused by a large electric field. Figure 7 shows time evolution of f in the middle layer during one period for the case, $L=5$ μm and $f_{\mathrm{req}}=200$ Hz, obtained from the numerical simulation. Significant amount of fluctuation is observed and such behavior must affect the inner-layer solutions through the higher-order effect as addressed by Bazant *et al.* [24]. In addition, the results shown in Fig. 7 are obtained by imposing $f=g=1$ rather than $\partial f/\partial Y=\partial g/\partial Y=0$ at $Y=Y_m$ in order to reduce the error. With this modified boundary condition, $\varepsilon_{\mathrm{rms}}$ is reduced to 6.9%, half of the previous result. On the other hand, for the parameter set giving the highest error in Fig. 6(a), the LHS of Eq. (27) is calculated to be $\varepsilon_1 V_{00}^*/\varsigma^*=3.9$, while for the case of Fig. 7 it is $\varepsilon_1 V_{00}^*/\varsigma^*=7.8$. Although the magni-

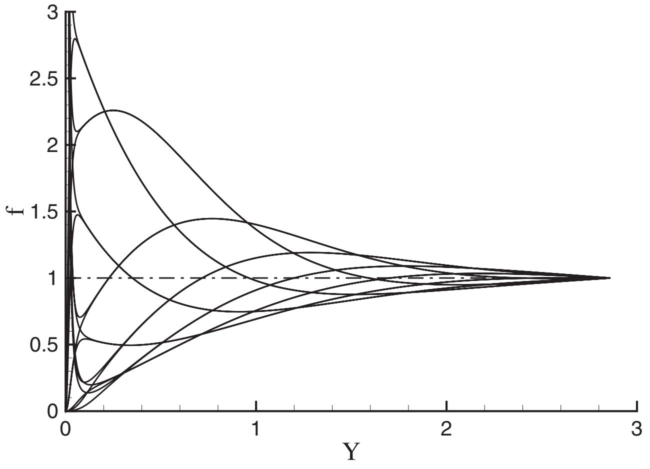

FIG. 7. Time evolution of profile of the concentration f obtained from the numerical simulation at 16 instants of time during one period in the middle layer with $L=5$ μm, $f_{\mathrm{req}}=200$ Hz, $c_0^*=c_{0A}^*$, and $V_{00}^*=0.8$ V.

tudes are larger than 1, the errors of the asymptotic solutions are not so much large; this means that the criterion Eq. (27) required for the present solution to be valid is too restrictive.

As is well known, the Debye-Hückel linear solutions are powerful because they provide a simple boundary condition on the electrode surface in solving the Laplace equation (5) for the bulk potential. Furthermore, because they are based on the assumption that temporal change of all the variables follows the same mode as the external one differing only in phase, it suffices to solve Eq. (5) once and for all without need to integrate it in a temporal sequence. But before employing a linear solution in an engineering application, we always raise the question as to how accurate the solution will be for the application at hand. For the current model problem, it can be shown that the Debye-Hückel linearization leads to the solution

$$\phi = \frac{V_{00}}{1+Q^2}\Bigg[\cos t - Q\sin t + \frac{\sqrt{\gamma}}{Y_m}\exp(-\sqrt{4\gamma}Y)(\sin t + Q\cos t)\Bigg],$$

where the constant Q is defined as

$$Q = \frac{\sqrt{\gamma}+2\gamma\varepsilon_2}{Y_m}.$$

This solution is of course valid for $\gamma \ll 1$; note that this corresponds to a linear regime, whereas our main interest in this paper lies in the nonlinear regime for $\gamma \gg 1$.

Figure 8 presents the time evolution of the potentials obtained by the asymptotic and Debye-Hückel approximation in comparison with that given by the numerical method at the parameter set, $L=10$ μm, $f_{\text{req}}=200$ Hz, and $c_0^*=c_{0A}^*$. At a low voltage $V_{00}^*=0.05$ V, Fig. 8(a), both the Debye-Hückel and asymptotic methods produce almost indistinguishably accurate results; the rms error was found to be $\varepsilon_{\text{rms}}=0.013$ and 0.003 for the Debye-Hückel and asymptotic methods, respectively. At a high volgate $V_{00}^*=0.8$ V, Fig. 8(b), the Debye-Hückel method overestimates the potential drop significantly, while the asymptotic solution shows considerable nonlinearity but very good agreement with the numerical solution. We obtained in this case $\varepsilon_{\text{rms}}=0.39$ for the Debye-Hückel solution, which is much larger than that given by the asymptotic method, $\varepsilon_{\text{rms}}=0.058$. The rms error of the Debye-Hückel solution turns out to be still large, $\varepsilon_{\text{rms}}=0.29$, at an increased spacing $L=100$ μm. It was found that, for this parameter set, the error of the linear solution is very small near $Y=0$, but it increases rapidly as distance from the electrode surface is increased. This implies that the error is caused by the overestimation of the potential drop across the inner layer with the given parameter set.

V. DISCUSSION ON MULTIPLE-LAYER STRUCTURE

We have shown that the dynamics of ion transport within the thin layer near the electrode surface under ac in the nonlinear regime can be explained in terms of quadruple-layer model including the Stern, inner, middle and outer layers, which can describe even the transient phenomenon. Since this structure is unique for ac against dc, we may call this the "dynamic electrical-quadruple-layer" (DEQL) model. The outer layer vanishes after the initial transient state. Therefore, when the steady (not static) state is of our only concern as usual, the term "dynamic electrical-triple-layer" (DETL) should be appropriate. The main difference between our DETL model and the classical EDL model lies in the existence of the middle layer outside the inner layer in DETL. Figure 1 illustrates the most important of the characteristics contained in each of these four layers, i.e. the difference in the dynamical range of the cation's concentration. Needlessly to say, in general the inner layer is far much thinner and the magnitude of the concentration is far larger than this figure shows. Also shown in this figure is the order of each layer's thickness in terms of the dimensional parameters. The order of the middle-layer thickness is the same as $O(\lambda_{\text{dif}})$, where λ_{dif} is defined as Eq. (4).

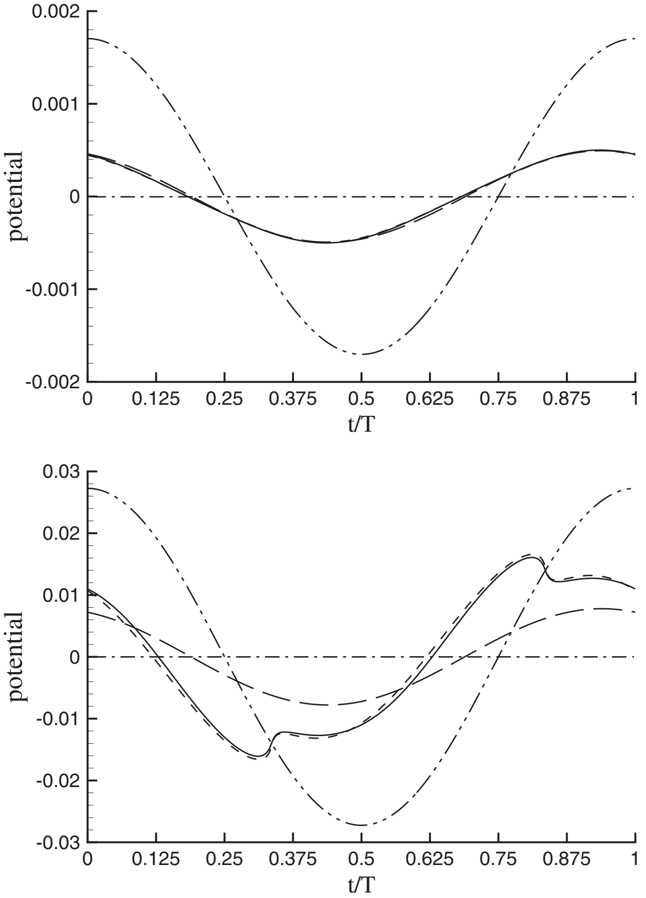

FIG. 8. Time evolution of potentials outside the inner layer (at $Y=0.0184$) obtained during the 20th period from the numerical simulation (solid line), asymptotic analysis (dashed), and Debye-Hückel linear analysis (long-dash) at $L=10$ μm, $f_{\text{req}}=200$ Hz, $c_0^*=c_{0A}^*$, and two different external potentials (dash-dot-dot line); (a) $V_{00}^*=0.05$ V; (b) $V_{00}^*=0.8$ V.

The inner layer in DETL corresponds to the "diffuse layer" in the EDL. However we assert that use of "diffuse layer" instead of the "inner layer" in the DETL is not reasonable considering the present solution structure. In many practical cases where a static disturbance is given in the form of dc or a constant zeta potential and the steady state is the only concern, the diffuse layer in the EDL model shows distribution of ionic concentrations determined by the balance between the diffusion and conduction effects, and the outside of the EDL is occupied by the neutralized bulk. The term "diffuse layer" therefore must be understood as a word used to represent the unique role of diffusion in this layer as a counteractive transport against the conduction. However, for the case with ac, the diffusion term is also dominantly important in the middle layer. Therefore, assigning "diffusion layer" to either the inner or outer layer may bring forth confusion and misunderstanding. On the other hand, the most diffusive action can be found in the outer layer during the transient period because it shows slow spreading of the concentrations throughout the layer; such diffusive spreading has been also predicted by Bazant *et al.* [24] for the transient problem under dc. Therefore, "diffusion layer" should be given to the outer layer of DEQL, if necessary.

As a suitable term for the middle layer, we may use "buffer" layer, in view of its role as an intermediate storage place in between the inner layer and the bulk (or the outer layer for the transient case). The potential drop occurs mostly across the Stern and inner layers in our DETL model, because both cations and anions are neutralized in the middle layer. Furthermore, its magnitude can be determined without resorting to the middle layer's dynamics. Therefore as far as the potential drop and its subsequent effect, i.e., slip velocity, are concerned, we do not need to consider the middle layer. However, it should play an important role when a higher-order correction to the present asymptotic solutions is considered in strongly nonlinear cases, i.e., at much higher V_{00} and γ and much lower ω to the extent that Eq. (27) is violated. Bazant *et al.* [24] also implied the existence of this kind of layer, called the depletion zone, but the zone soon disappeared and merged into the outer layer and then into the bulk. As indicated in Fig. 5, the magnitude of the conduction flux within the middle layer is larger than that of the diffusion flux. So, we may be tempted to think that the conduction term has the same importance as the diffusion term in the middle layer (contrary to our pre-assumption for the middle-layer analysis). However, this is not correct, because the conduction flux is spatially uniform while the diffusion flux is not, as shown in Fig. 5; that is, the gradient of the conduction flux which appears in the Nernst-Planck equation becomes zero and so can be neglected.

Existence of the middle layer was also implied by Dukhin and Shilov from Ukrainan school for the steady [30,31] and unsteady [32] external forcing. They proposed the governing equation in the same form as Eq. (26) and presented the solutions for the case of ion transport around a spherical particle. However, no double-frequency oscillation was confirmed in the their solutions [32]. Olesen [33] also presented the asymptotic analysis to the ion transport in the three layers outside the Stern layer (Debye, diffusion and bulk in their terms) for the weakly and strongly nonlinear regimes but without ion adsorption. For the case of the weakly nonlinear regimes, we have checked that his formula (2.137) is equivalent to ours (23). Our analysis is however unique in that we presented a fairly accurate prediction of the ion transfer through each layer by using a very simple formula like Eqs. (37) and (38). Discussion presented in this paper by using the quantitative analysis provides very clear insight into the ion transport process. The problem of using unsuitable terminology concerning the multiple-layer structure has also been raised in this paper, which should be a benchmark for further discussion on the standardization. In addition, we have presented the range of errors to be expected from the asymptotic solutions. Finally, we proposed the asymptotic analysis to the ion transport problem when the ion adsorption is included, its specific effects being presented in the following section.

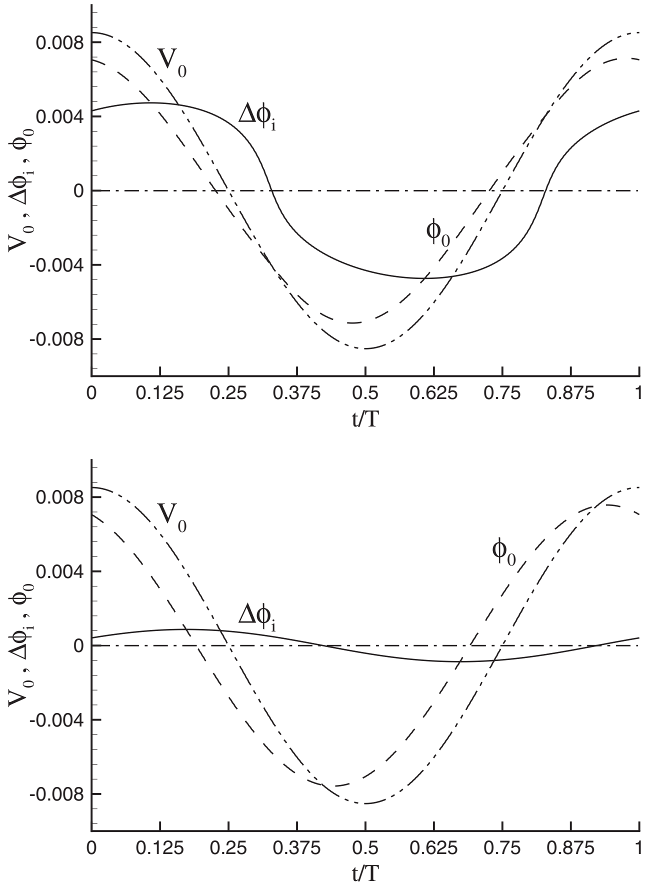

FIG. 9. Time evolution of the potential drop across the inner layer $\Delta\phi_i$ (solid lines) and the potential at the interface ϕ_0 (dashed) obtained from the asymptotic solution together with the external potential V_0 (dash-dot-dot) applied at the electrode; (a) without adsorption ($\Gamma_{max}=\alpha=0$); (b) with adsorption at $\Gamma_{max}=5$ and $\alpha=0.2$. Basic parameters are $L=20$ μm, $f_{req}=200$ Hz, $c_0^*=c_{0A}^*$, and $V_{00}^*=0.25$ V.

VI. EFFECT OF THE ION ADSORPTION

We now address the effect of the ion adsorption on the solution of the ion-transport equations. When adsorption occurs at the interface between the Stern and inner layers, the ion concentrations within the inner layer must be decreased which in turn should result in the decrease of the potential drop across the inner layer, $\Delta\phi_i$, as shown in Fig. 9(b) for the case of ion adsorption in contrast with Fig. 9(a) for the case

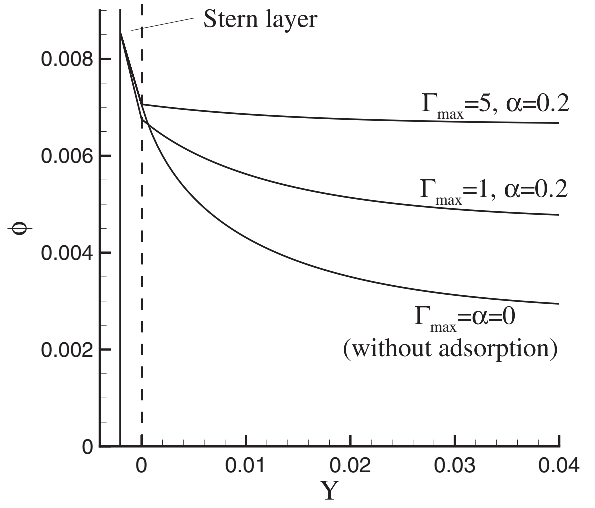

FIG. 10. Potential distribution at $t=0$ obtained from the asymptotic solution for the case without adsorption and two cases with adsorption. Other parameters are the same as in Fig. 9. Vertical solid and dashed lines correspond to the electrode surface and the interface between the Stern layer and the inner layer, respectively.

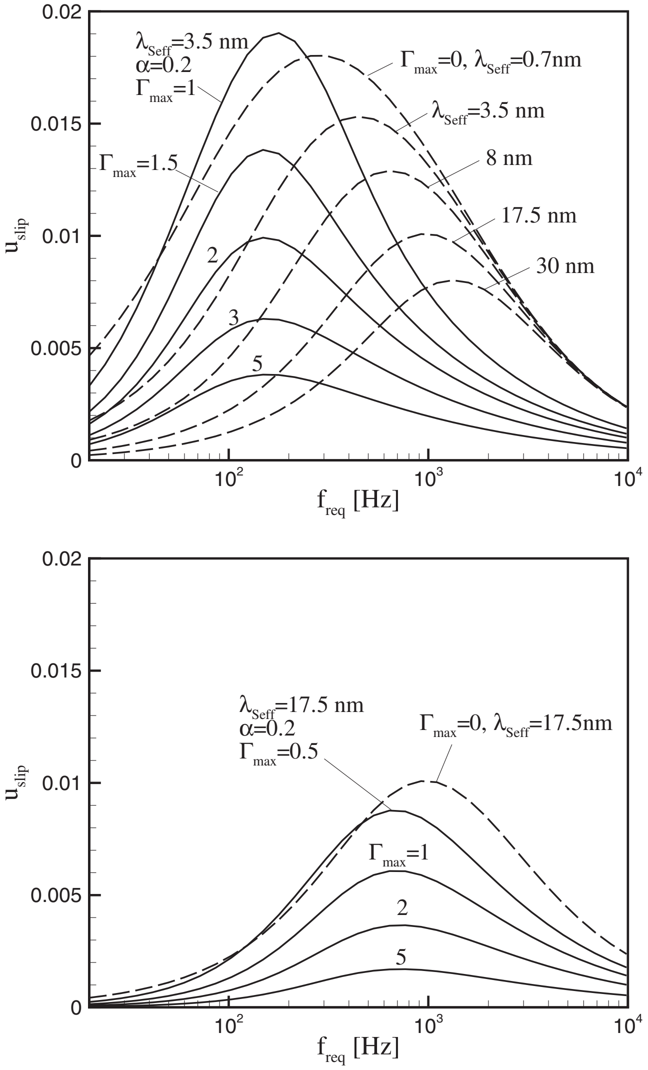

FIG. 11. Effect of the ion adsorption on the dimensionless virtual slip velocity, u_{slip}, as a function of the ac frequency; solid lines are for the case of ion adsorption with different values of $\Gamma_{\max}$ at (a) $\alpha=0.2$ and $\lambda_{\mathrm{Seff}}=3.5$ nm and at (b) $\alpha=0.2$ and $\lambda_{\mathrm{Seff}}=17.5$ nm; dashed lines are for the case without ion adsorption. Other parameters are the same as in Fig. 9.

without ion adsorption. The amount of potential drop within the Stern layer however cannot be intuitively predicted. Figure 10 shows the instantaneous potential distribution at $t=0$ obtained from the asymptotic solution for the two cases with ion adsorption in comparison with one without adsorption. It reveals that the amount of the Stern-layer potential drop is not so much changed with the adsorption. This means that the magnitude of the potential at the outer edge of the inner layer, ϕ_∞, must increase when the adsorption occurs.

The effect of the ion adsorption on the electrokinetics should manifest itself as the change of slip velocity. It can be shown that the steady slip-velocity u^*_{slip} at the outer edge of the inner layer along a tangential, x^* direction caused by the potential drop within the inner layer is given from

$$u^*_{\mathrm{slip}} = \frac{\varepsilon\varepsilon_0}{\mu}\left\langle \Delta\phi^*_i \frac{\partial\phi^*_\infty}{\partial x^*}\right\rangle,$$

where μ is viscosity of the bulk electrolyte and the symbol $\langle\,\rangle$ denotes the time average. In deriving this formula we assumed that the adsorbed ions are immobile along the tangential direction. For the case of parallel facing electrodes, the potential ϕ^*_∞ is uniform over the plane parallel to the electrode surface leading to $\partial\phi^*_\infty/\partial x^*=0$, and so no fluid motion is expected to occur in this case. Otherwise when ϕ^*_∞ varies on the plane, the slip velocity is proportional to $\Delta\phi^*_{\mathrm{i}}$ and $\partial\phi^*_\infty/\partial x^*$, and we can estimate the order of magnitude of the latter by ϕ^*_∞/L. So, we can define a virtual slip velocity for the case of parallel facing electrodes as follows:

$$u^*_{\mathrm{slip}} = \frac{\varepsilon\varepsilon_0 s^{*2}}{\mu L}u_{\mathrm{slip}},$$

where u_{slip} is the dimensionless "virtual" slip velocity defined as

$$u_{\mathrm{slip}} = \gamma^2\langle\phi_\infty\Delta\phi_i\rangle. \tag{39}$$

The idea implied by the introduction of the virtual slip velocity is to indirectly catch the effect of the ion adsorption on the slip velocity for the general case of non-parallel electrodes.

Figure 11 shows the dependence of u_{slip}-frequency curves on the effective Stern-layer thickness λ_{Seff} for the case without adsorption, $\Gamma_{\max}=\alpha=0$, and that on the maximum available areal concentration $\Gamma_{\max}$ at $\lambda_{\mathrm{Seff}}=3.5$ nm and $\alpha=0.2$ in Fig. 11(a) and at $\lambda_{\mathrm{Seff}}=17.5$ nm and $\alpha=0.2$ in Fig. 11(b). Without exception, each of the curves exhibits a critical frequency at which the slip velocity becomes maximum. For the case of coplanar electrodes, theory has always overpredicted the experimental measurement as for the slip velocity up to one or two order of magnitude [5,6,8,11,25]. Increase of $\lambda_{\rm Seff}$ gives rise to decrease of the maximum slip velocity, but the critical frequency shifts to higher values as shown in Fig. 11(a). This then results in overprediction of the critical frequency. When the ion adsorption is included, maximum slip velocity increases with $\Gamma_{\max}$ at low values of $\Gamma_{\max}$ as shown in Fig. 11(a) (compare the dashed curve of $\Gamma_{\max}=0$ and $\lambda_{\rm Seff}=3.5$ nm with the solid curve of $\Gamma_{\max}=1$ and $\lambda_{\rm Seff}=3.5$ nm); this kind of unexpected increase of the slip velocity at low values of $\Gamma_{\max}$ seems to be due to the momentary increase of the magnitude of ϕ_∞. At $\Gamma_{\max}$ high enough, i.e., for $\Gamma_{\max}>1$, $u_{\rm slip}$ decreases monotonically with $\Gamma_{\max}$ as shown in Fig. 11(a). Remarkably, the critical frequencies are now much smaller than the case without adsorption. Although the results for adsorption in Fig. 11(a) are obtained with fixed $\lambda_{\rm Seff}$ and α, adjustment of these parameters should produce a lot of variation in the magnitude of $u_{\rm slip}$ as well as the critical frequency. For instance, Fig. 11(b) presents an example at $\lambda_{\rm Seff}=17.5$ nm, and it indeed reveals that the critical frequencies are higher than in Fig. 11(a). Applying the present asymptotic theory including the ion adsorption to the case of nonparallel electrodes must be interesting but is beyond the scope of the present study.

VII. CONCLUSIONS

We have shown, with the aid of asymptotic analysis and numerical simulation, that the ion-transport equations intrinsically contain triple-layer or quadruple-layer solutions at large values of the parameter γ, when the layer is receiving ac potential. Excluding the Stern layer, the inner layer is the thinnest and the concentrations develop in time with a strongly nonharmonic behavior. The concentrations of the positive and negative ions show the temporal behaviors at the same frequency as the external one with the time-phase difference of a half period from each other leading to the corresponding potential drop. In the middle layer, both the positive and negative ion concentrations develop in the same magnitude and same time phase, and so no potential drop occurs. This layer can be considered as a reservoir or buffer supplying ions to or receiving them from the inner layer and bulk (or outer layer) depending on their demand during a period. This give-and-take process results in the temporal oscillation of the concentrations with a period double the forcing one. The outer layer is characterized by a slow diffusion of the excess concentrations which were initiated by the initial conditions or the nonzero steady components developed from the beginning in the inner layer. In this layer too, no potential drop is expected, because the positive and negative ion concentrations show identical behavior. After the transient period this layer vanishes and is absorbed into the bulk.

We have shown that nonspecific adsorption of ions at the interface between the Stern and inner layers can exert considerable influence on the virtual slip-velocity depending on the corresponding parameter values. Since, for a given amount of ion transport from the buffer zone, the ion concentrations spread in the inner layer are decreased due to the adsorption, the potential drop in the inner layer must decrease, and this in turn leads to the lower slip velocity at the outer edge of the inner layer.

In the near future we will apply the present method to the calculation of the slip velocity on a pair of coplanar electrodes under ac and compare the solutions with the experimental data presented by Green *et al.* [8]. We also have a plan to study the improvement of the solutions given in this paper for the case of large fluctuation of concentrations in the middle layer. To take this effect into consideration, we may need to add some other dynamic variables or pertinent equations. Development of numerical schemes that consider the steric effect [26,34] of the concentrations on the potential drop may also be a good subject of future study. We also plan to deliberate on including the ion transport along the tangential direction on the electrode surface as tried by Chu and Bazant [27].

ACKNOWLEDGMENTS

This work was supported by the Korea Science and Engineering Foundation (KOSEF) through the National Research Laboratory Program funded by the Ministry of Science and Technology (No. 2005-1091).

---

[1] D. Li, *Electrokinetics in Microfluidics* (Elsevier Academic Press, New York, 2004).
[2] M. Trau, D. A. Savile, and I. A. Aksay, Langmuir **13**, 6375 (1997).
[3] N. G. Green and H. Morgan, J. Phys. D **31**, L25 (1998).
[4] A. Ramos, H. Morgan, N. G. Green, and A. Castellanos, J. Phys. D **31**, 2338 (1998).
[5] A. Gonzalez, A. Ramos, N. G. Green, and A. Castellanos, Phys. Rev. E **61**, 4019 (2000).
[6] M. Scott, K. V. I. Kaler, and R. Paul, J. Colloid Interface Sci. **238**, 449 (2001).
[7] M. Scott, R. Paul, and K. V. I. Kaler, J. Colloid Interface Sci. **230**, 377 (2000).
[8] N. G. Green, A. Ramos, A. Gonzalez, H. Morgan, and A. Castellanos, Phys. Rev. E **66**, 026305 (2002).
[9] P. K. Wong, C.-Y. Chen, T.-H. Wang, and C.-M. Ho, Anal. Chem. **76**, 6908 (2004).
[10] P. K. Wong, T.-H. Wang, J. H. Deval, and C.-M. Ho, AIEEE/ASME Trans. Mech. **9**, 366 (2004).
[11] M. R. Brown and C. D. Meinhart, Microfluid. Nanofluid. **2**, 513 (2006).
[12] H. Zhou, L. R. White, and R. D. Tilton, J. Colloid Interface Sci. **285**, 179 (2005).
[13] J. Wu, Y. Ben, D. Battigelli, and H.-C. Chang, Ind. Eng. Chem. Res. **44**, 2815 (2005).
[14] J. Wu, Y. Ben, H.-C. Chang, Microfluid Nanofluid **1**, 161 (2005).
[15] M. Lian, N. Islam, and J. Wu, J. Phys.: Conf. Ser. **34**, 589 (2006).
[16] K. H. Bhatt, S. Grego, and O. D. Velev, Langmuir **21**, 6603

(2005).

[17] K. F. Hoettges, M. B. McDonnell, and M. P. Hughes, J. Phys. D **36**, L101 (2003).

[18] Z. Gagnon and H.-C. Chang, Electrophoresis **26**, 3725 (2005).

[19] M. Mpholo, C. G. Smith, and A. B. D. Brown, Sens. Actuators B **92**, 262 (2003).

[20] V. Studer, A. Pepin, Y. Chen, and A. Ajdari, Microelectron. Eng. **61-62**, 915 (2002).

[21] M. Z. Bazant and T. M. Squires, Phys. Rev. Lett. **92**, 066101 (2004).

[22] T. M. Squires and M. Z. Bazant, J. Fluid Mech. **560**, 65 (2005).

[23] S.-C. Wang, Y.-W. Lai, Y. Ben, and H.-C. Chang, Ind. Eng. Chem. Res. **43**, 2902 (2004).

[24] M. Z. Bazant, K. Thornton, and A. Ajdari, Phys. Rev. E **70**, 021506 (2004).

[25] J. A. Levitan, S. Devasenathipathy, V. Studer, Y. Ben, T. Thorsen, T. M. Squires, and M. Z. Bazant, Colloids Surf., A **267**, 122 (2005).

[26] M. S. Kilic, M. Z. Bazant, and A. Ajdari, Phys. Rev. E **75**, 021503 (2007).

[27] K. T. Chu and M. Z. Bazant, Phys. Rev. E **74**, 011501 (2006).

[28] C. S. Mangelsdorf and L. R. White, J. Chem. Soc., Faraday Trans. **94**, 2441 (1998).

[29] C. S. Mangelsdorf and L. R. White, J. Chem. Soc., Faraday Trans. **94**, 2583 (1998).

[30] S. S. Dukhin and V. N. Shilov, Colloid J. USSR **32**, 564 (1969).

[31] S. S. Dukhin and V. N. Shilov, Adv. Colloid Interface Sci. **13**, 153 (1980).

[32] V. N. Shilov and S. S. Dukhin, Colloid J. USSR **32**, 90 (1970).

[33] L. H. Olesen, Ph.D. thesis, Technical University of Denmark, 2006.

[34] I. Borukhov, D. Andelman, and H. Orland, Phys. Rev. Lett. **79**, 435 (1997).